Phase Space Gradient Driven Discrete Compressional Alfvén Eigenmodes in Tokamaks: Simulations and Observations[1]

N. N. Gorelenkov 1), C. Z. Cheng 2), N. A. Crocker 3), E. D. Fredrickson 1), W. W. Heidbrink 4), S. Kubota 3), C. K. Phillips 1), W. A. Peebles 3), G. Wang 3)

1) Princeton Plasma Physics Laboratory, Princeton University, Princeton, NJ, USA 08543
2) National Cheng-Kung University, Taiwan
3) University of California, Los Angeles, CA, USA
4) University of California, Irvine, CA, USA.

e-mail contact of main author: ngorelen@pppl.gov

Abstract. The spectrum of Compressional Alfvén Eigenmodes (CAE) driven by phase space gradient measured in NSTX and DIII-D plasmas is analyzed numerically (more details can be found in Ref.[1]). Advanced diagnostic capabilities made it possible to measure single mode polarization and toroidal mode numbers, which unambiguously identifies studied modes to be of compressional branch. CAE modes form the discrete spectrum with each mode having three (quantum) mode numbers (M, S, n), where M, S, and n are poloidal, radial and toroidal mode numbers, respectively. CAE mode frequency splitting corresponding to change of each of these mode numbers seem to be observed in experiments and is consistent with our numerical analysis. CAE mode structure is computed to be localized in both radial and poloidal directions and is shown to be consistent with the internal reflectometer diagnostic data.

Multiple CAEs, if excited either internally or externally with sufficient amplitude, are expected to channel energy from fusion products or other fast ions to heat thermal ions [2, 3]. CAEs are reported to drive the plasma current in rotomak experiments [4] and can be potentially used for energetic particle and plasma diagnostic.

The existence of localized Compressional Alfvén Eigenmodes (CAEs, also called fast Alfvén or magnetosonic eigenmodes) was predicted in cylindrical geometry [5, 6] which have dispersion and polarization given approximately by $\omega = kv_A$, where v_A is the Alfvén velocity at the mode location, k is the characteristic wavevector, $k_\theta \equiv m/r \sim k$, where m is the characteristic poloidal harmonic number, r is the minor radius of the magnetic surface. These modes and their localization were suggested to be critical in order to explain the Ion Cyclotron Emission (ICE) from the plasma driven by superalfvenic energetic ions [7] (and in such works as [8–10]). In Ref. [11] poloidal localization of CAEs was predicted and was required for CAE instabilities to minimize their damping.

New experimental insights into the CAE physics were offered in more recent studies in the National Spherical Torus experiment (NSTX) where these modes were shown to be excited in new regimes with the mode frequencies at a fraction of the thermal ion cyclotron frequency

[1] *This research was supported in part by the U.S. Department of Energy under the contract DE-AC02-76CH03073*

$0.3f_{ci} < f < f_{ci}$ [12–15]. It was demonstrated that the instability frequencies correlate with the plasma Alfvén velocity. In the very recent similarity experiments between NSTX and DIII-D, CAEs were observed in DIII-D by lowering the equilibrium magnetic field to achieve the same ratio of the Alfvén velocity to the beam injection velocity [16]. Similar magnetic activity was observed in the Mega Ampere Spherical Tokamak (MAST) [17]. These recent experiments on NSTX, MAST and DIII-D renewed interest in the CAE theory mainly because observed CAE spectra exhibit discrete modes well separated in frequencies due to the relatively low magnetic field used in experiments. Advanced diagnostic capabilities made it possible to measure single mode polarization and mode numbers [12, 14], which unambiguously identified observed modes to be of the compressional branch. We note that in addition to CAEs, the instabilities of the shear Alfvén branch eigenmodes called global Alfvén eigenmodes (GAEs), were seen on the magnetic spectra in the same frequency range [3]. GAEs could be easily separated from CAEs by the characteristic magnetic spectrum intersections of their signal peaks as the safety factor evolvs in time, whereas the spectral lines of CAEs never intersect.

Limited numerical studies were published to confirm theoretical findings by solving the CAE envelop equations such as in Refs. [11, 18]. Most recently, global calculations with the use of the wave codes did find a localized CAE solution for the highest possible toroidal mode numbers, n (at fixed mode frequency) [19], whereas simulations did not show any localization of the CAEs at low n's. The eigenmode localization seems to be less critical for the instabilities in NSTX, but appears to be favorable for the CAE instability because injected mostly passing beam ions interact more efficiently with such modes due to outboard radial deviation of their drift trajectories at the low field side of the plasma cross section.

We are performing the numerical study of the CAE spectrum and structure in order to verify theoretical predictions. We use global ideal MHD code NOVA [20].

1. High frequency mode observations in NSTX

Both edge magnetic pick-up coil and reflectometer diagnostics have observed high, up to thermal ion cyclotron frequency, coherent plasma oscillations in NSTX [12, 13]. Observations showed broad and complicated frequency spectra of coherent modes between $400kHz$ and up to $2.5MHz$, with the fundamental cyclotron frequency of background deuterium ions to be $f_{cD0} = \omega_{cD}/2\pi = 2.3MHz$, calculated at the vacuum magnetic field at the geometrical axis of NSTX for $B_{g0} = 0.3T$ [12]. In experiments the Alfvén velocity was varied by controlling the magnetic field and plasma density, which resulted in correlation with the mode frequencies. Typically the range of operational parameters for the experiments are: toroidal current $I_p = 0.7 - 1MA$, $B_{g0} = 0.3 - 0.45T$, central electron density $n_{e0} = 1 - 5 \times 10^{13} cm^{-3}$, central electron temperature of up to $T_{e0} = 1keV$. CAEs were observed only in plasmas heated by a deuterium beam with a power of $P_b = 1.5 - 3MW$. The typical magnitude of the perturbed magnetic field at the plasma edge is small $\delta B_{\|}/B \sim 10^{-6}$ [12].

New capabilities of the magnetic pick up coil Mirnov diagnostic include the possibility to measure the mode number and the polarization of the magnetic field oscillations [14]. We show the magnetic spectrum at high frequency for NSTX discharge $\#117521$ in figure 1 with the following

plasma parameters: $B_{g0} = 0.44T$, major radius at the geometrical center $R_0 = 0.85m$, minor radius of the last magnetic surface in the equatorial plane $a = 0.61m$, $n_{e0} = 5.83 \times 10^{13} cm^{-3}$, $f_{cD0} = 3.39MHz$, whereas at the edge $f_{cDedge} = 2.67MHz$. The polarization of three particular modes measured near the plasma edge clearly illustrate that these modes are of the compressional branch since $\delta B_{\|} > \delta B_{\perp}$. Measurements of the toroidal mode number often give low- to medium-n's. In the example shown in the figure, the low band of modes at $0.5 < f[MHz] < 1$ has mostly positive low toroidal mode numbers $-1 \leq n < 7$, whereas the higher frequency band, $1.6 < f[MHz] < 2.2$ is characterized by rather high negative toroidal mode numbers, n changing sequentially from -9 to -13 as the mode frequency goes up. Positive n means that the mode is propagating against the plasma current.

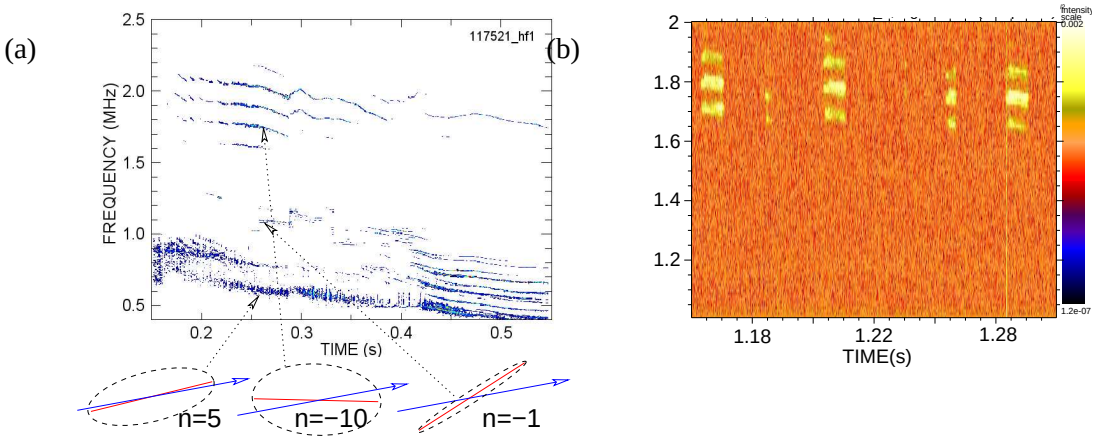

FIG. 1: High frequency magnetic field oscillation spectrum evolution during NSTX discharge $\#117521$ (figure (a)) and during DIII-D discharge $\#122806$ (figure (b)). Shown also are the results of the polarization measurements for three compressional type oscillations in NSTX (figure (a)). Each polarization sub-figure has an ellipse, which is the trace of the perturbed magnetic field vector, and an arrow, which shows the direction of the equilibrium magnetic field.

2. CAE observations in DIII-D

In experiments on DIII-D [16] plasma conditions, similar to those in NSTX were created to investigate conditions for high frequency instabilities in conventional tokamaks. NSTX and DIII-D plasmas differ only in major radii, $R_0 = 1.67m$ in DIII-D ($a = 0.61m$). High frequency observations at $f \sim f_{ci}/2$ in conventional tokamaks were not reported before. When the magnetic field was lowered to such a value that beam ions are superalfvenic, high frequency instabilities appear with the similar properties observed in NSTX. Qualitatively, observations agree with the theory, but some discrepancies remain. An example of the magnetic spectrum is shown in figure 1 (b) for the DIII-D similarity experiment plasma shot $\#122806$, which was chosen out of an experimental database in which both reflectometer and magnetic pick up coils diagnostics were available and showed similar spectra. The modulation in the signal is due to the modulation in the applied beam injection. Unfortunately the identification of the toroidal mode numbers and the polarization of the measured magnetic activity was not possible within the campaign.

3. Compressional Alfvén eigenmode modeling by MHD code NOVA

Additional plasma profiles for one NSTX and one DIII-D discharge of interest, the safety factor, $q(r)$, and the normalized plasma density, $\bar{n} \equiv n(r)/n(0)$, are shown in figure 2.

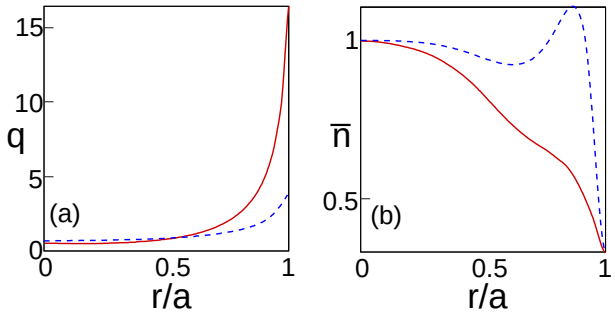

FIG. 2: NSTX shot $\#117521$, $t = 0.5sec$ and DIII-D shot $\#122806$, $t = 1.205$ safety factor (figure (a)) and normalized density (figure (b)) profiles. Solid curves correspond to NSTX plasma, whereas dashed curves correspond to DIII-D plasma. Safety factor values (figure (a)) in the center are 0.706 and 0.982 in NSTX and DIII-D, and 16.3 and 3.02 at the edge, respectively.

For the simplicity, allow for the wavelength to be small in comparison to the equilibrium scale lengths and write the dispersion of the compressional branch in the form $\omega^2 = v_A^2 \nabla^2$, where we also implied that the plasma pressure is small and $\omega^2/\omega_{ci}^2 \ll 1$. If there is a direction of symmetry, such as along the cylinder axis or around the torus in the tokamak plasma we can write

$$\left(\nabla_\perp^2 - k_\varphi^2 + \frac{\omega^2}{v_A^2} \right) \xi = 0, \tag{1}$$

where φ is the toroidal (symmetry) angle, the subscript $\perp$ means that the derivative operator is applied in the direction perpendicular to $\nabla\varphi$, and plasma displacement ξ is chosen as the perturbed quantity. It is clear from this equation that the combination $k_\varphi^2 - \omega^2/v_A^2 \equiv V$ plays the role of an effective potential of the eigenmode problem. The variation of V in the plasma cross section perpendicular to the direction of symmetry comes from both the Alfvén velocity, $v_A^2 = B^2/4\pi\rho_{pl}$, where ρ_{pl} is the plasma mass density, and the toroidal wavevector, $k_\varphi = n/R$, where R is the major radius, and n is the toroidal mode number. In finite aspect ratio plasma V typically has poloidal minimum at the low field side (LFS) due to B poloidal variation. It is clear that if n is high, k_φ term helps to localize the wave like region at the LFS and is argued to be the reason for poloidal localization of high-n CAEs [19]. Summarizing our heuristic theory, the frequency of CAEs is expected to be described by this equation

$$\omega_{MSn}^2 \simeq v_A^2 \left(\frac{M^2}{r^2} + \frac{S^2}{L_r^2} + \frac{n^2}{R^2} \right), \tag{2}$$

where all relevant values should be taken at the minimum of V, S is the radial quantum number, L_r is the characteristic radial width of the effective potential, and M is the generalized poloidal quantum number, which is the same as a single poloidal harmonic number, m, only for the cylindrical geometry. In general case CAE solution has a single M, but should be expanded in several

poloidal m harmonics. Hence, it is expected that each eigenmode corresponds to a unique combination (M, S, n).

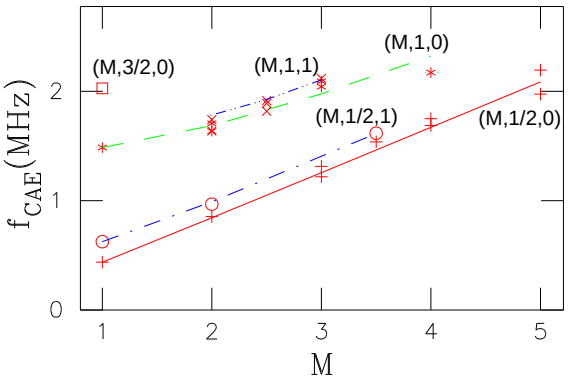

FIG. 3: CAE spectrum (shown in MHz) in DIII-D computed with the non-monotonic density profile from figure 2. Shown are different radial bands (S number) for $n = 0$ and $n = 1$, and $S = 1/2, 1, 3/2$ as marked.

The experimentally measured density profile of DIII-D plasma is non-monotonic as shown in figure 2 (b). As a result the effective potential has two minima and two solutions with the same mode numbers and similar mode structures, but slightly different eigenfrequencies. Hence, the computed CAE spectrum looks more complicated as shown in figure 3, where curves correspond to M^2 dependence for each band and at given M two solutions are shown as points marked identically (where they were found). The difference in frequency due to such "density profile" splitting is quite small, $\Delta\omega/\omega = 1 - 5\%$. As an example we show the structure (see figure 4 (a) and (b)) of CAEs split in frequency due to this "density profile" effect for $M = 2$, $S = 1$, and $n = 0$. As expected split modes are slightly shifted radially (in this example by $\Delta r/a \simeq 3\%$) and are somewhat differently represented by the poloidal harmonics.

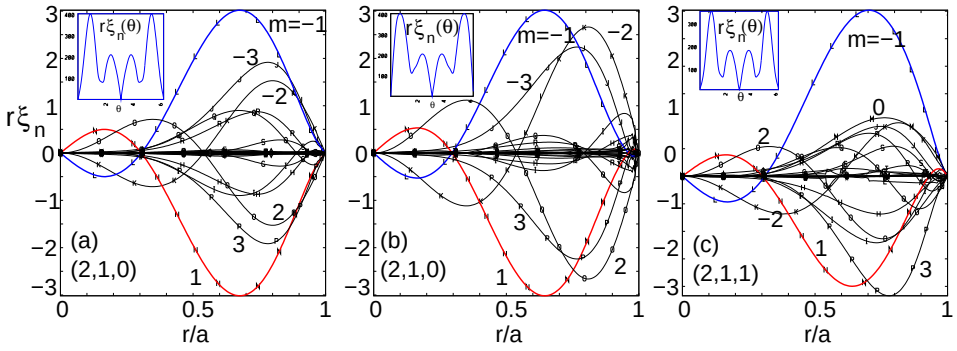

FIG. 4: CAE mode structures for $(2, 1, 0)$ mode split in two solutions, (a) and (b), due to the non-monotonic density profile shown in figure 2. (c) Shows the mode $(2, 1, 1)$, which is asymmetric in sign of m due to $n \neq 0$. Inserts at the top left corner of each graph show the poloidal dependence of each mode.

The NSTX CAE spectrum (Figure 5) has similar properties to the one calculated for DIII-D. However, finding the CAE solutions for NSTX plasma turns out to be more challenging due to stronger poloidal harmonic coupling. Within one radial (or S) band we observe eigenmode splitting even for the used monotonic density profile. In addition, the numerically clearly identifiable lowest radial band contains several eigenmodes at given M. These mode can exist due to the geometrical effect of STs [21]. The other notable difference with the DIII-D spectrum is that in NSTX radial bands tend to be more dense in frequency for high M. In Figure 6 an example of the radial and poloidal structures of $(5/2, 1, 0)$ CAE mode in NSTX is shown.

4. Comparisons with experiment

In the experiments on DIII-D n was not measured and only two reflectometer channels were available, so that detailed comparisons with NOVA modeling seems to be difficult. On the other hand, in NSTX not only toroidal mode numbers but the mode polarizations were measured. Three fixed-frequency quadrature O-mode reflectometers launch microwaves into the plasma at 30, 42 and 50 GHz, which allows for simultaneous measurements of the plasma oscillations at three radial points. Changes in the relative phase of the launched and reflected microwaves are measured and used to estimate density fluctuation levels at the cutoff making use of the phase screen model [22].

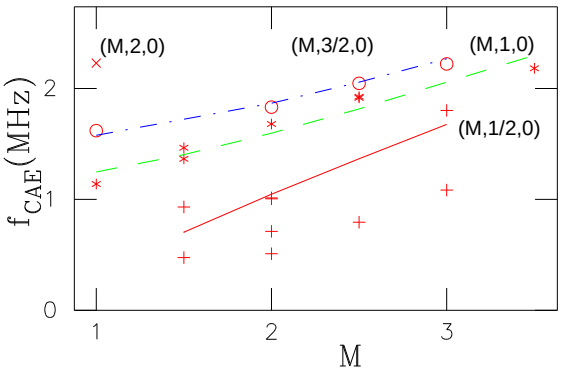

FIG. 5: CAE spectrum in NSTX with the same notations as in figure 3, but only for $n = 0$, and $S = 1/2, 1, 3/2, 2$ as marked.

We choose the low-n mode with compressional polarization, which is persistent in time from $t = 0.25sec$ to $t = 0.55sec$ and is shown as having $n = -1$ in figure 1 (a). By the time of modeling $t = 0.5sec$ its frequency was $f = 0.81MHz$. The closest mode in frequency, which reveals similar mode structure has $f = 0.93MHz$ and $(3/2, 1/2, 0)$. The results of the comparison are shown in figure 7. Note that the level of the density fluctuations is $\delta n/n \simeq 2 \times 10^{-4}$ at the peak of the reflectometer signal for this mode. One can see from figure 7 that the profile of the normal component of the plasma displacement and the density perturbation are quite different, which indicates that the compressional effects are important.

In earlier publications on CAE observations [12, 13], it was pointed out at three characteristic frequency separations between different observed instabilities, which concluded from the data analysis and its comparison with the theory. Different frequency separation scales (frequency splittings) also follow from our numerical results as presented in figures 3 and 5. They are associated with the CAE frequency variation when one of three mode numbers is changed. If we denote Δf_j to be the frequency variation due to the change in $j = M$, S, or n, we can deduce from the simulated spectra that in DIII-D one expects (see figure 3 (b)) $\Delta f_S = 0.7 - 1\,MHz$, $\Delta f_M = 200kHz$ for $S = 1/2$, $\Delta f_M = 120kHz$ for $S = 1$, and $\Delta f_n \simeq 50kHz$. Although the CAE spectrum in DIII-D shown in figure 1 (b) contains only a few modes, recently reported results in similar experiments with more rich CAE spectra [16] imply the following $\Delta f_S \simeq 1MHz$, $\Delta f_M \simeq 130kHz$, $\Delta f_n \simeq 30kHz \pm f_{rot}$, $f_{rot} \simeq 20kHz$. This seems to be in reasonable agreement with our results. More accurate comparison does not seem possible at the moment because all three numbers have to be measured simultaneously.

In NSTX, our simulations predict for frequency splitting $\Delta f_S = 0.5 - 1\,MHz$, $\Delta f_M = 200kHz$, $\Delta f_n = 50kHz$. Whereas for the shot $\#117521$ (figure 1 (a)) we find $\Delta f_S \simeq 1MHz$, $\Delta f_M \simeq 120kHz$, $\Delta f_n \simeq 20kHz \pm f_{rot}$, $f_{rot} \simeq 20kHz$. Note that for the n splitting, we took the smallest frequency separation, which may be also due to the nonmonotonic density profile or other geometrical effects.

The main discrepancy with the theory [23, 24] is in the toroidal mode number splitting at low-n, and M numbers. It is surprising that the simulations are in better agreement with the simple heuristic dispersion (see Eq.(2)), which can be reduced to $\Delta f_n/f \sim nr^2/R^2M^2$. The poloidal mode number dependence of CAE eigenfrequency is close to the parabolic in both theories.

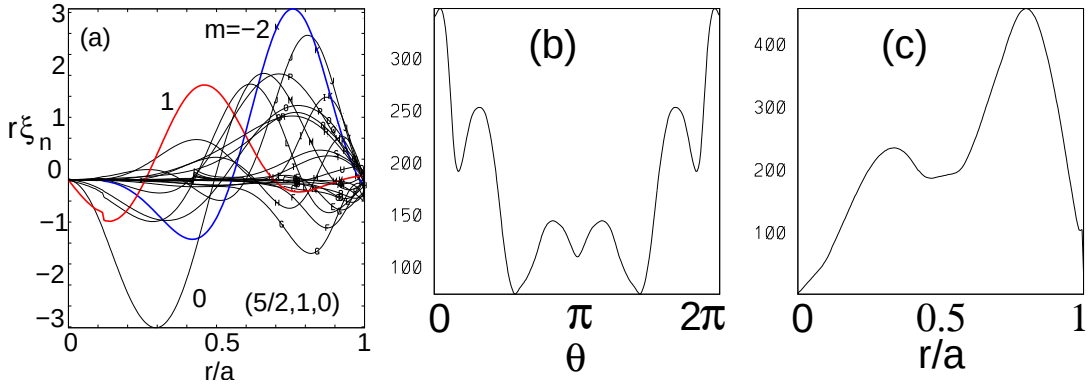

FIG. 6: $(5/2, 1, 0)$ CAE radial structure in NSTX (a) and its radial rms $\langle r\xi_n \rangle_r (\theta)$ (b) and poloidal rms $\langle r\xi_n \rangle_\theta (r)$ (c).

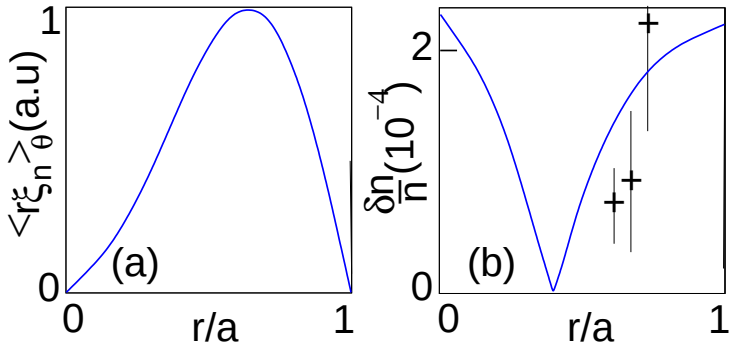

FIG. 7: $(3/2, 1/2, 0)$ CAE plasma displacement (a) in the midplane on the LFS in NSTX. (b) Shows density perturbation in the midplane. Points marked with plus signs correspond to experimental data from the reflectometer diagnostic. Shown also are the error bars for each point.

5. Summary

We have shown that the measurements of the magnetic field polarization help to identify unambiguously sub-cyclotron oscillations as CAEs. The ideal MHD code NOVA is capable of simulating low-n CAEs and is enable to confirm poloidal and radial localization of these modes in NSTX and DIII-D predicted earlier by theory. This may be important for the development of the CAE instability theory. Numerically calculated eigenmodes can be used for accurate evaluation of the CAE growth rates with such codes as NOVA-K [25].

Geometrical effects are shown to be important for the simulation of the CAE mode structure and spectrum. Simulations also show that the theory qualitatively captures main properties of CAEs. Still, some aspects such as toroidal mode number frequency splitting are not well described in

analytical theory. It seems to be important to include ω/ω_c corrections in terms of the Hall term as well as FLR effects.

We also would like to emphasize that observed CAE modes in NSTX belong to the same branch responsible for the ICE instabilities in tokamaks with higher aspect ratio, which may however exist at a fraction of the fundamental ion cyclotron frequency. These modes are suggested to be responsible for the anomalous energy diffusion of beam ions in TFTR experiments [26].

[1] N. Gorelenkov, E. Fredrickson, W. Heidbrink, N. Crocker, S. Kubota, and W. Peebles, Nucl. Fusion **46**, S933 (2006).
[2] D. Gates, N. N. Gorelenkov, and R. B. White, Phys. Rev. Lett. **87**, 205003 (2001).
[3] N. N. Gorelenkov, E. D. Fredrickson, E. Belova, C. Z. Cheng, D. Gates, S. Kaye, and R. B. White, Nucl. Fusion **43**, 228 (2003).
[4] Y. Petrov, F. Zhong, and T. S. Huang, Phys. Plasmas **12**, 082514 (2005).
[5] S. M. Mahajan and D. W. Ross, Phys. Fluids **26**, 2561 (1983).
[6] B. Coppi, S. Cowley, R. Kulsrud, P. Detragiache, and F. Pegoraro, Phys. Fluids **29**, 4060 (1986).
[7] B. Coppi, Phys. Lett. A **172**, 439 (1993).
[8] N. N. Gorelenkov and C. Z. Cheng, Phys. Plasmas **2**, 1961 (1995).
[9] V. S. Belikov, Y. I. Kolesnichenko, and O. A. Silivra, Nuclear Fusion **35**, 1603 (1995).
[10] T. Fülöp, Y. I. Kolesnichenko, M. Lisak, and D. Anderson, Nucl. Fusion **37**, 1281 (1997).
[11] N. N. Gorelenkov and C. Z. Cheng, Nucl. Fusion **35**, 1743 (1995).
[12] E. D. Fredrickson, N. N. Gorelenkov, C. Z. Cheng, R. Bell, D. Darrow, D. Johnson, S. Kaye, B. LeBlanc, J. Menard, S. Kubota, et al., Phys. Rev. Lett. **87**, 145001 (2001).
[13] N. N. Gorelenkov, C. Z. Cheng, E. D. Fredrickson, E. Belova, D. Gates, S. Kaye, G. J. Kramer, R. Nazikian, and R. B. White, Nucl. Fusion **42**, 977 (2002).
[14] E. D. Fredrickson, N. N. Gorelenkov, and J. Menard, Phys. Plasmas **11**, 3653 (2004).
[15] N. N. Gorelenkov, E. Belova, H. L. Berk, C. Z. Cheng, E. D. Fredrickson, W. W. Heidbrink, S. Kaye, and G. J. Kramer, Phys. Plasmas **11**, 2586 (2004).
[16] W. W. Heidbrink, E. D. Fredrickson, N. N. Gorelenkov, T. Rhodes, and M. A. VanZeeland, Nucl. Fusion **46**, 324 (2006).
[17] L. C. Appel, R. J. Akers, T. Fülöp, R. Martin, and T. Pinfold, in *Proceedings of 31th European Physical Society Conference on Plasma Physics*, London, England, 2004, edited by Prof. R. M. Pick, P. Helfenstein (European Physical Society, CCLRC Rutherford Appleton Laboratory and Euratom/UKAEA Fusion Association Culham Laboratory, 2004) **28G**, 4.195 (2004).
[18] T. Fülöp, M. Lisak, Y. I. Kolesnichenko, and D. Anderson, Phys. Plasmas **7**, 1479 (2000).
[19] T. Hellsten and M. Laxøaback, Phys. Plasmas **10**, 4371 (2003).
[20] C. Z. Cheng, Phys. Reports **211**, 1 (1992).
[21] M. V. Gorelenkova and N. N. Gorelenkov, Phys. Plasmas **5**, 4104 (1998).
[22] R. Nazikian, G. J. Kramer, and E. Valeo, Phys. Plasmas **8**, 1840 (2001).
[23] N. N. Gorelenkov, C. Z. Cheng, and E. Fredrickson, Phys. Plasmas **9**, 3483 (2002).
[24] H. Smith, T. Fülöp, M. Lisak, and D. Anderson, Phys. Plasmas **5**, 1437 (2003).
[25] N. N. Gorelenkov, C. Z. Cheng, and G. Y. Fu, Phys. Plasmas **6**, 2802 (1999).
[26] D. S. Clark and N. J. Fisch, Phys. Plasmas **7**, 2923 (2000).